



Defluoridation of aqueous solutions by nanocomposite of $MgAl_2O_4$ and MA-VA-AA polymer: kinetics and mechanism

Muhammad Aslam Malana*, Javaria Dost Muhammad, Muhammad Naeem Ashiq, Ruqiyah Sehrish Gohar

Institute of Chemical Sciences, Bahauddin Zakariya University, Multan 60800, Pakistan, Tel. +92 61 9210092; email: draslammalana@gmail.com (M.A. Malana), Tel. +92 332 0656080; email: jdostmuhammad@yahoo.com (J.D. Muhammad), Tel. +92 300 9879344; email: naemashiqqau@yahoo.com (M.N. Ashiq), Tel. +92 333 6140303; email: ruqiyah_4444@hotmail.com (R.S. Gohar)

Received 25 December 2013; Accepted 16 May 2014

ABSTRACT

A nanocomposite of co-precipitatively synthesized $MgAl_2O_4$ and methyl acrylate-vinyl acetate-acrylic acid polymer was prepared through radical polymerization mechanism. The synthesized material was characterized by XRD, TGA, DSC, and SEM. XRD analysis of magnesium aluminate confirms the single spinel phase with average crystallite size of 33 nm. Adsorption of fluoride on the nanocomposite was studied at 308 K. The adsorption data were fitted to Freundlich, Langmuir, and Flory–Huggins models. Better correlation and comparable values of theoretical and experimental adsorption capacities (q_e) indicated that the adsorption process followed pseudo-second-order kinetics. Mechanism of the adsorption process was investigated by applying Bingham's and intraparticle diffusion models. Deviation from linearity of Bingham's plot and significant value of intercept obtained from intraparticle diffusion model showed that both the film diffusion and pore diffusion processes may be the rate-controlling steps. Moreover, 96% successful removal of the fluoride by the synthesized nanocomposite, suggest it to be a suitable adsorbent for defluoridation of aqueous solutions.

Keywords: Fluoride removal; Nanocomposite; Adsorption; Magnesium aluminates; Kinetics and mechanism

1. Introduction

Fluoride in drinking water may be beneficial as well as detrimental depending upon its concentration [1]. When present in the significant amount it is considered as essential component for normal mineralization of bones, formation of dental enamel, and prevention of dental carries [2]. Beyond the permissible limit (1–1.5

mg/L) it causes various disorders and diseases such as crippling, skeletal fluorosis, brittle bones, lung and bladder cancer, infertility in women, brain and hepatic damage, and Alzheimer syndrome [3–5]. To prevent fluoride related diseases the exposed population has to be provided with safe drinking water.

Various sources such as glass manufacture, electroplating operations, pesticides, fertilizer semiconductor, steel, and aluminum industries contribute significantly in fluoridation of water [6]. Fluorine is highly reactive

*Corresponding author.

and is found naturally as CaF_2 . It is an essential constituent in minerals like topaz, fluorite, fluorapatite, cryolite, and phosphorite and can be leached out by rain water, thereby contaminating ground and surface waters [7]. Ground water with high-fluoride concentration is reported in Pakistan, India, West Africa, Thailand, China, Sri Lanka, Iraq, Iran, Sudan, Ethiopia, Uganda, Kenya [8], and USA.

Various treatment procedures have been reported for the removal of excess fluoride from water. These can be classified into precipitation [9], nanofiltration [10], electrodialysis [11], and adsorption [12,13]. Adsorption is still widely accepted pollution removal technique due to its ease of operation and cost effectiveness [12,14,15]. This method involves the passage of contaminated water through an adsorbent bed, where fluoride is removed by physical, ion exchange or surface chemical reaction with adsorbent. Researchers have used different types of adsorbents such as fired clay, brick powder, cotton cellulose, spent bleaching earth, activated carbon, zeolite, red mud, quick lime, silica, polymer, etc. [16–18]. Fluorine being a highly electronegative element has extraordinary tendency to get attracted by positively charged ions like aluminum and alkali metals [19] so, alumina is frequently used for the removal of fluoride from water [18,20].

In this work, we have attempted to synthesize a nanocomposite (methyl acrylate (MA)-vinyl acetate (VA)-acrylic acid (AA) polymer with nanomagnesium aluminate) and used it as an adsorbent for the removal of fluoride from aqueous media. As the adsorption phenomenon is directly related to the surface area of adsorbent, the efficiency of polymer as an adsorbent may be enhanced by doping them with nanomagnesium aluminate. This composite (nanomagnesium aluminate doped polymer) may have higher binding capacity for fluoride, when exposed to fluoride solution of different concentrations (due to porosity and larger surface area). The adsorption kinetics and mechanism have also been discussed in the present studies.

2. Materials and methods

2.1. Chemicals

Chemicals used in the preparation of MgAl_2O_4 and the nanocomposite were as follows: aluminum nitrate, $\text{Al}(\text{NO}_3)_3 \cdot 9\text{H}_2\text{O}$ (Merck, 98%), magnesium nitrate, $\text{Mg}(\text{NO}_3)_2 \cdot 6\text{H}_2\text{O}$ (Merck, 100%), as starting materials for the synthesis of magnesium aluminate, NH_3 (Riedel Dehaen) as precipitating agent, methacrylate, $\text{CH}_2=\text{CHCOOCH}_3$ (Merck, 99%), vinyl acetate, $\text{CH}_2=\text{CHOCOCH}_3$ (Fluka, 99%), acrylic acid, CH_2CHCOOH (Fluka, 99%) as

monomers for the synthesis of the copolymer, span 80 reagent for fluoride assessment (HACH, CAT# 444-53, lot # A9008), chloroform, CHCl_3 (Fluka, 100%) as porogen, ethylene glycol dimethyl acrylate, $\text{CH}_2=\text{C}(\text{CH}_3)\text{C}(\text{O})\text{OCH}_2\text{CH}_2\text{OC}(\text{O})\text{C}(\text{CH}_3)=\text{CH}_2$ (Fluka, 100%) as a cross-linking agent, ethanol, $\text{CH}_3\text{CH}_2\text{OH}$ (Merck and 99% purity) as a solvent and benzoyl peroxide, $(\text{C}_6\text{H}_5\text{CO})_2\text{O}_2$ (Fluka, 100%) as an initiator. All these chemicals were used as such without further treatment.

2.2. Synthesis of magnesium aluminate nanomaterial

Magnesium aluminate nanomaterial was synthesized by the chemical co-precipitation method [21]. The solutions of desired concentrations (1:2 ratio of Mg and Al) for $\text{Mg}(\text{NO}_3)_2 \cdot 6\text{H}_2\text{O}$ and $\text{Al}(\text{NO}_3)_3 \cdot 9\text{H}_2\text{O}$ were mixed in a beaker with constant stirring for half an hour. The reaction mixture was heated up to 323 K and 2.0 M ammonia solution was added drop wise to the reaction mixture for precipitation with continuous vigorous stirring. Addition of NH_3 solution was continued until the pH of solution reached between 10 and 11. The reaction temperature was maintained for 3 h. Then the precipitates were washed with deionized water until pH of solution becomes neutral (to remove NH_3 and other water soluble impurities). The product was dried in an oven at 393 K to remove water contents. The dried powder was finally annealed in box furnace (Heraeus, D-6450 Hanau, Germany) at 1,073 K for 8 h to obtain the pure single phase.

2.3. Preparation of nanocomposite

The monomers (MA-VA-AA) used were taken in the volumetric ratio of 2.5:1:2.5. Both the chloroform as porogen and EGDMA as cross-linking agent were taken 50% *v/v* of the total monomers volume. All the chemicals were mixed in a 250 mL quick-fit (double neck) flask equipped with condenser. Ethanol (50 mL) and benzoyl peroxide (1% *w/v* of the total volume) were added to the reaction mixture as solvent and initiator, respectively. An optimized amount of 0.2 g of synthesized MgAl_2O_4 nanomaterial was then added in this mixture. The radical polymerization process was carried out following slow heating scheme [22]. The reaction mixture was continuously stirred at 303–343 K. After each increment of 5 K, the temperature was maintained for at least 1 h. The precipitation was started at 335 K and the polymerization process was completed at 343 K. The precipitates were separated by filtration and washed with ethanol and then with deionized water to remove unreacted material. The product was dried in an oven at 373 K and grounded in agate pestle and

mortar to convert it into fine powder. This powder was then used as an adsorbent for removal of fluoride from aqueous solutions.

2.4. Adsorption studies

A stock solution of 1,000 mg/L of fluoride was prepared by dissolving required amount of NaF (99.99%, Aldrich) in deionized water. The solutions of 2, 4, 6, 8, 10, 12, and 14 mg/L were prepared by further dilution of the stock solution with the same solvent. For adsorption studies, 25 mL of the solution of the given fluoride concentration and an optimized amount of adsorbent (0.2 g) was shaken in an orbital shaker at 308 K for 90 min. The residues were separated by filtration and the filtrates were analyzed for fluoride concentration by SPAND indicator method. In this method, 1 mL of spand reagent was added to 10 mL of the test solution. The reaction mixture was shaken and kept for one minute to allow the reaction to complete (colour development). Fluoride concentration in this solution was then measured at 580 nm by using UV–visible spectrophotometer (Analytik JENA SECORD 200). The amount of fluoride adsorbed on nanocomposite was calculated using the following equation (Eq. (1)):

$$q_e = (C_0 - C_e) \frac{V}{m} \quad (1)$$

where C_0 is the initial fluoride ion concentration (mg/L), C_e is the equilibrium concentration (mg/L), V is the solution volume (L), and m is the mass (g) of nanocomposite.

2.5. Characterization

Thermal analysis was performed by a Perkin Elmer (TGA/DTA diamond series) thermal analyzer from 303 to 1,373 K at the heating rate of 5 K/min. Powder X-ray diffraction analysis was carried out by Philips X'Pert PRO 3040/60 diffractometer which uses Cu $K\alpha$ as a radiation source. Scanning electron microscope (Jeol JSM-6490A) was used to visualize the surface morphology of $MgAl_2O_4$, the polymer, and the nanocomposite before and after adsorption of fluoride.

3. Results and discussion

3.1. Characterization of nano $MgAl_2O_4$

TGA curve for unannealed sample of $MgAl_2O_4$ shows weight loss in the first region (333–473 K) corresponding to the removal of water and volatile

material. The weight loss in the second region (473–573 K) can be ascribed to the removal of hydrated water and NH_3 adsorbed in the layers of the synthesized sample. Weight loss in the third region (573–773 K) can be attributed to the conversion of metal hydroxides into metal oxides. The residual amount of 51% is of metal oxides which remain stable over the temperature range studied.

The DSC curve of this sample is in good agreement to the TGA curve. It shows the endothermic peaks at 373, 553, and 773 K corresponding to the evaporation of water and volatile components, removal of hydrated water and ammonia adsorbed in layers, and the conversion of metal hydroxides to metal oxides, respectively.

XRD pattern of $MgAl_2O_4$ is depicted in Fig. 1. This pattern was indexed as single spinel phase when compared with JCPDS Card No. 21-1152. No extra peak is observed which indicates that there is no impurity in the synthesized sample. The average crystallite size for the synthesized sample was calculated by the Scherer's formula (Eq. (2)) [23]:

$$D = \frac{k\lambda}{\beta \cos \theta} \quad (2)$$

where λ is wavelength of incident X-rays (i.e. 1.541 Å), β is full width at half maxima, θ is Bragg's angle, K is Scherer's constant. The average crystallite size is found to be 33 nm.

The SEM image of $MgAl_2O_4$ shows that the surface of the material is smooth and the particles are uniformly distributed. All the particles look spherical in

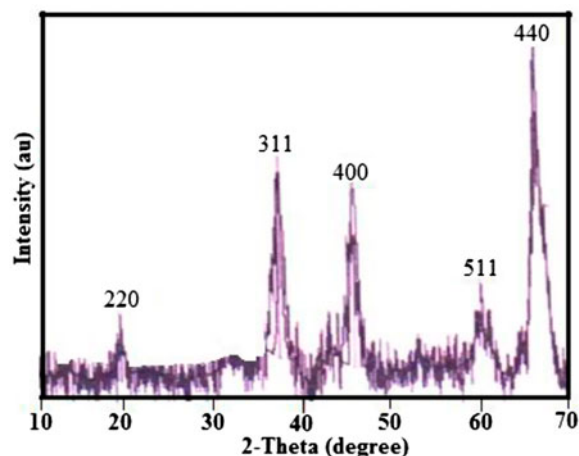


Fig. 1. XRD pattern for $MgAl_2O_4$ synthesized by the chemical co-precipitation method.

shape and the surface look porous which is beneficial for the adsorption process. The approximate particle size as shown in this image is in the range of 15–35 nm which is in agreement with that of calculated from XRD data.

3.2. Characterization of nanocomposite

TG/DTG curve of MgAl_2O_4 -polymer composite (Fig. 2) shows total weight loss of 96% in the temperature range of 473–793 K. The first weight loss occurred at 473–523 K which can be assigned to the removal of hydrated water from the sample. The weight loss at 533–663 K (84%) corresponds to the decomposition of organic matters in the synthesized sample. The final weight loss at 663–793 K indicates the oxidation of backbone of the polymer chain of the sample. The residual amount of 3.2% is that of the doped MgAl_2O_4

in the polymer which is stable at this temperature range.

The SEM image of MA-VA-AA polymer shows that all the particles are spherical in shape and linked with each other. The particle size calculated from SEM is in the range of 250–300 nm. The SEM micrograph of nanocomposite before fluoride adsorption (Fig. 3(a)) shows average particle size in the range of 15–40 nm. The particles of MgAl_2O_4 are embedded in to the porous surface of the polymer. There are pores present on the surface of the nanocomposite which act as active sites for the adsorption of fluoride. The SEM image of nanocomposite after fluoride adsorption is also shown in Fig. 3(b). This shows that the pores present on surface of the composite are filled and the surface is saturated with fluoride ions and looks smooth which indicates that the fluoride is adsorbed on the surface of the nanocomposite.

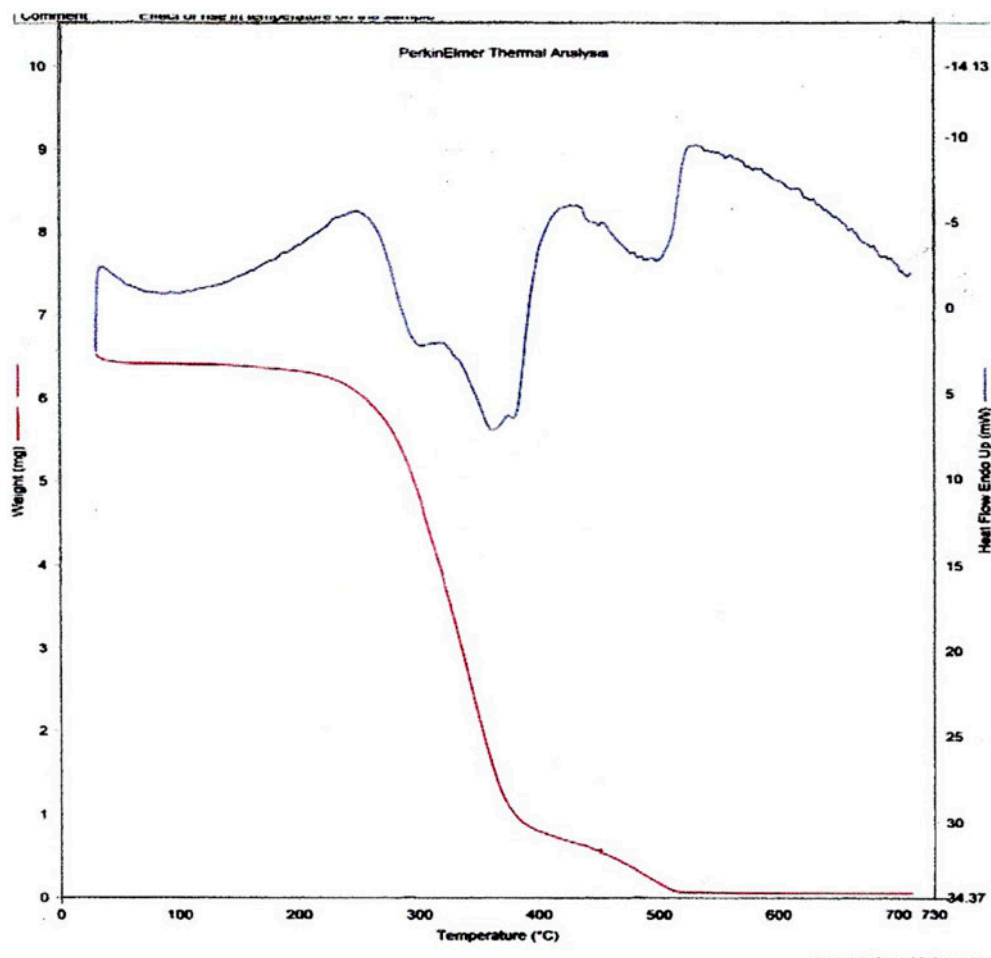


Fig. 2. TG/DTG Curve of MgAl_2O_4 -polymer (MA-VA-AA) nanocomposite.

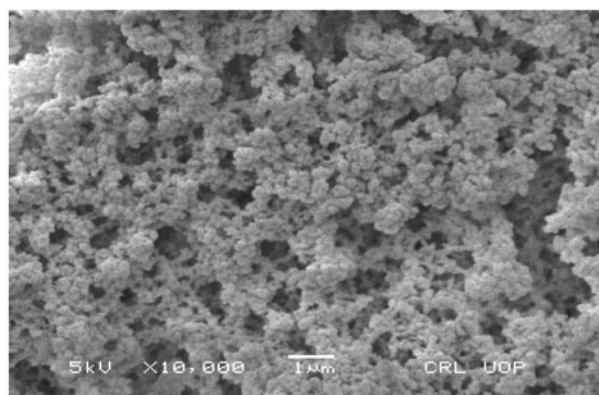


Fig. 3(a). SEM image of the nanocomposite before adsorption.

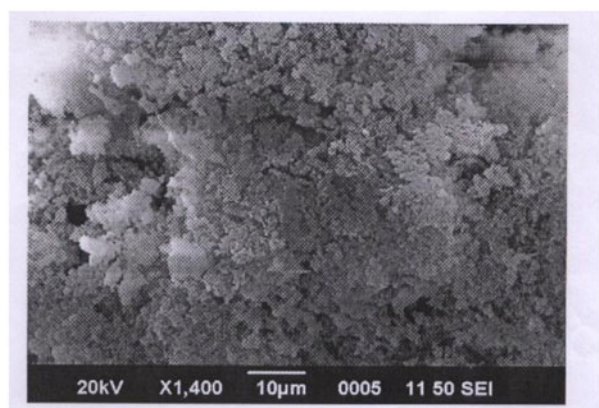


Fig. 3(b). SEM image of the nanocomposite after fluoride adsorption.

3.3. Effect of solution pH on fluoride adsorption

The effect of solution pH on fluoride adsorption was investigated in the pH range of 2–6 at given fluoride concentration (10 mg/L) and is shown in Fig. 4. The adsorption of fluoride on the nanocomposite increases with the increase in pH value and obtains maximum value of q_e at pH 4.0. Above pH 4.0 the amount of fluoride adsorbed on the surface of nanocomposite decreases. The pK_a value for acrylic acid is 4.25 and above pH 4.0 the deprotonation of the acrylic acid in the polymer started which causes repulsion between carboxylate ions of the polymer and fluoride ions. Consequently, the adsorption of fluoride on the nanocomposite decreases at higher pH. It is noticed that at lower pH the adsorption of fluoride on the nanocomposite is less. This may be attributed to the leaching of magnesium aluminates in to the aqueous solution at more acidic pH [8] thereby decreasing the quantity of adsorbent in the medium.

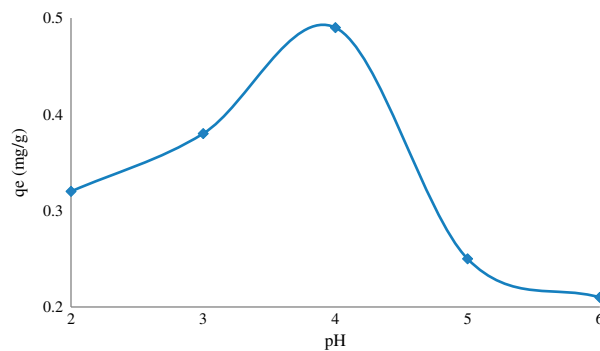


Fig. 4. Variation of amount of fluoride adsorbed on the nanocomposite as a function of solution pH.

3.4. Percentage removal of fluoride from aqueous solutions

Fluoride being highly electronegative is capable of making stronger hydrogen bonds with water, thus making defluoridation of water more difficult particularly at low-fluoride concentrations (less than 10 mg/L). In the present studies, it is observed that percentage removal of fluoride on the nanocomposite increases with decreasing fluoride concentration in solution and shows 96% fluoride removal for the fluoride concentration of 2.7 mg/L. This behavior is an indication of the fact that the synthesized nanocomposite can effectively be used as an adsorbent at lower fluoride concentration in solution.

3.5. Adsorption isotherms

3.5.1. Equilibrium isotherm

The plot of q_e (amount of adsorbate adsorbed per gram of the adsorbent) vs. concentration of adsorbate depicts the L-type adsorption isotherm. Long plateau as obtained in the isotherm can be explained in terms of degree of saturation and high-energy barrier that has to be overcome before adsorption occurs at new sites. The further rise in adsorption indicates the presence of newly developed bare surface upon which adsorption can occur.

3.5.2. Langmuir model

The linear form of Langmuir isotherm [24] is given in Eq. (3):

$$\frac{C_e}{q_e} = \frac{1}{K_L} + \frac{a_L}{K_L} C_e \quad (3)$$

The parameters K_L (L/g) and a_L (L/mg) are calculated from intercept and slope of the plot of C_e/q_e against

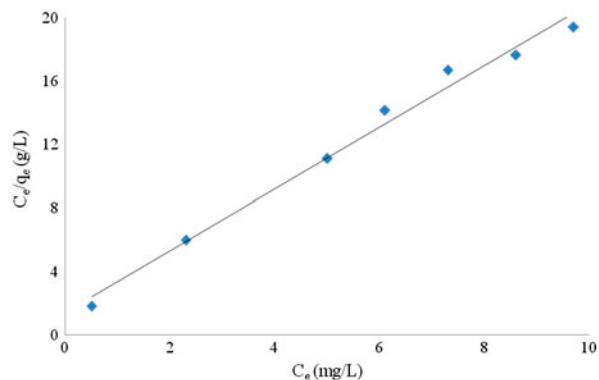


Fig. 5. Langmuir plot for the adsorption of fluoride on the nanocomposite.

C_e as shown in Fig. 5 and their values are given in Table 1. K_L and a_L are the Langmuir adsorption constants related to the energy of adsorption and binding forces between adsorbate and adsorbent, respectively. The value of a_L (Table 1) indicates that the binding forces are strong between adsorbate and adsorbent. The dimensionless factor R_L is calculated from Eq. (4) [24]:

$$R_L = \frac{1}{1 + \frac{a_L}{C_0}} \quad (4)$$

when R_L is greater than 1, adsorption is unfavorable and is favorable when R_L is greater than 0 and less than 1. When it is equal to zero then adsorption is irreversible and is linear when it is equal to 1. The value of R_L obtained in the present studies (Table 1) indicates that adsorption of fluoride on the nanocomposite is favorable.

Adsorption capacity (q_m) is the amount of adsorbate adsorbed per gram of the adsorbent and can be calculated using the following expression (Eq. (5)) [25]:

$$q_m = \frac{k_L}{a_L} \quad (5)$$

the adsorption capacity (q_m) for the adsorption of fluoride on the nanocomposite in the present investigation is higher (Table 1) than that of previous reported values (0.31 and 0.21 mg/g) [26] indicating that the synthesized nanocomposite can be used as an adsorbent for the removal of fluoride from the aqueous media.

3.5.3. Freundlich model

Adsorption data of fluoride on the nanocomposite are fitted to linear form of Freundlich isotherm (Eq. (6)) [27]:

$$\ln q_e = \ln K_f + \frac{1}{n} \ln C_e \quad (6)$$

where K_f is Freundlich constant and is associated with degree of adsorption and $1/n$ is heterogeneous factor which tells whether the adsorption process is favorable or not [28]. The parameters (K_f and $1/n$) calculated from the intercept and slope of plot $\ln C_e$ vs. $\ln q_e$, respectively, are given in Table 1. The value of $1/n$ for the adsorption of fluoride on the nanocomposite is less than unity showing that the process of adsorption is favorable. Comparing R^2 values for both the isotherms, it is concluded that Langmuir model is more appropriate to describe the adsorption data.

Table 1
Analysis of the results of adsorption of fluoride on the nanocomposite at 308 K

Parameters	Langmuir model	Freundlich model	FH model
a_L (L/mg)	1.348146	–	–
K_L (L/g)	0.694348	–	–
q_m (mg/g)	0.515039	–	–
$1/n$	–	0.197	–
K_f (mg/g)	–	0.317302	–
R_L	0.66697	–	–
n	–	–	1.0665
K_{FH} (L/mg)	–	–	0.0192
ΔG (kJ/mol)	–	–	–1.394
R^2	0.987	0.948	0.862

3.5.4. Flory–Huggins model

The F–H model was used to account for the degree of surface coverage characteristics of the adsorbate on the adsorbent [28]. Plot of $\log \theta/C$ against $\log (1-\theta)$ shown in Fig. 6 was plotted using Eq. (7):

$$\log \frac{\theta}{C} = \log K_{FH} + n \log(1 - \theta) \quad (7)$$

The parameters n and K_{FH} are obtained from the slope and intercept of the curve, respectively, and their values are tabulated in Table 1. The factor n shows the number of adsorbate occupying adsorption sites. The equilibrium constant (K_{FH}) is used to calculate the Gibbs free energy change (ΔG). The negative value of ΔG (-1.394 kJ/mol) indicates that the adsorption of fluoride on the nanocomposite is spontaneous [27].

3.6. Kinetic studies of adsorption

Kinetic studies of adsorption provide information about the efficiency as well as mechanism of the adsorption process. In the present studies, kinetics of fluoride adsorption on the nanocomposite were analyzed by applying pseudo-first-order (Eq. (8)) and pseudo-second-order (Eq. (9)) [29] kinetic models to the experimental data:

$$\ln (q_e - q_t) = \ln q_e - k_1 t \quad (8)$$

$$\frac{t}{q_t} = \frac{1}{k_2 q_e^2} + \frac{t}{q_t} \quad (9)$$

where k_1 and k_2 are the pseudo-first-order and pseudo-second-order rate constants, respectively. The

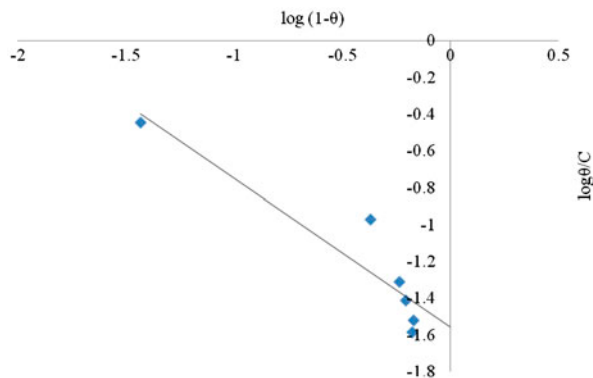


Fig. 6. Flory–Huggins plot for the adsorption of fluoride on the nanocomposite.

values of rate constants (k_1 and k_2) and adsorption capacity (q_e) obtained from slopes and intercept of these plots (Figs. 7 and 8), respectively, are listed in Table 2. The values of correlation coefficient (R^2) obtained for first-order kinetic model is lower than that obtained for the pseudo-second-order model (Table 2). Moreover, the q_e value as calculated from pseudo-second-order is in good agreement with experimental q_e value (Table 2). It is therefore, concluded that pseudo-second-order kinetic model provides a better fit to the experimental data.

3.7. Adsorption mechanism

Adsorption in general occurs in the following four steps:

- (1) Transfer of solute from bulk of the solution to the boundary layer (bulk diffusion);

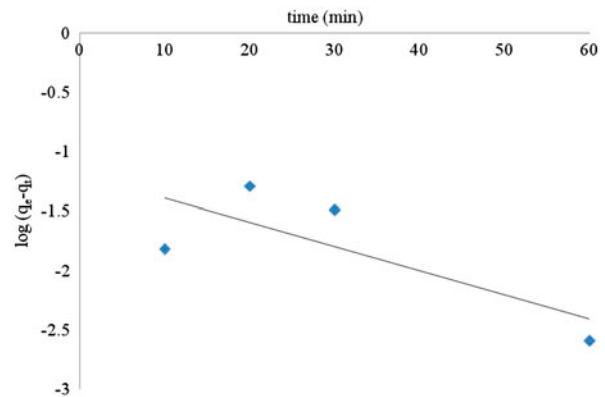


Fig. 7. Pseudo-first-order kinetic model for the adsorption of fluoride on the nanocomposite.

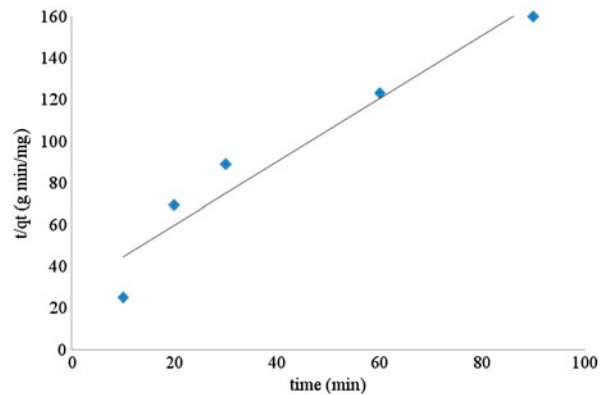


Fig. 8. Pseudo-second-order kinetic model for the adsorption of fluoride on the nanocomposite.

Table 2

The values of correlation coefficient (R^2), rate constants (k_1 and k_2), and adsorption capacity (q_e) calculated for pseudo-first-order and pseudo-second-order kinetic models

Order	R^2	q_e (mg/g)	k_1	k_2
Pseudo-first-order	0.590	0.0747	-0.0203	
Pseudo-second-order	0.932	0.658		0.0514

- (2) Transport of solute from boundary layer to the surface of the material (film diffusion);
- (3) Transfer of solute from adsorbent surface to active intraparticle sites (intra particle diffusion); and
- (4) Interaction between solute molecules and the available adsorption sites on the internal surface of the adsorbent.

Usually first and fourth steps are fast and the rate of reaction may depend upon second or third step. In order to investigate the rate-limiting step in the present studies; Bingham's model (Eq. (10)) as well as intraparticle diffusion model (Eq. (11)) was applied to the experimental data.

3.7.1. Bingham's model

Bingham's model (Eq. (10)) for the adsorption of fluoride on the nanocomposite is plotted as Fig. 9.

$$\log \left[\log \left(\frac{c_t}{c_0} - q_t m \right) \right] = \log k_0 + q_t \log t \quad (10)$$

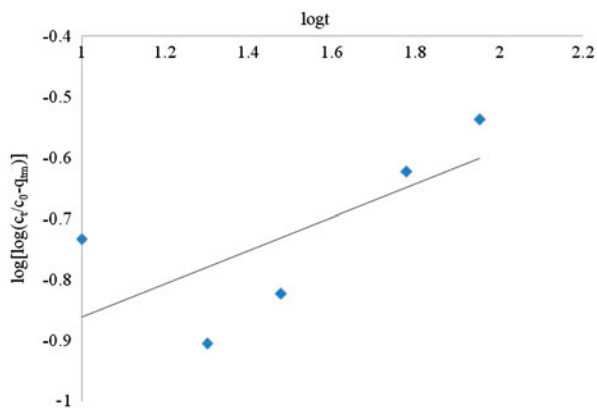


Fig. 9. Graph for the Bingham's equation for the removal of fluoride on the nanocomposite.

where C_0 is the initial concentration of adsorbate in solution, m is the mass of the nanocomposite per litre of solution, q_t is the amount of adsorbate at time t and k_0 is constant.

The poor correlation ($R^2 = 0.46$) shows unsatisfactory fit of this model thus, indicating that diffusion of the adsorbate into the pores of adsorbent is not the only rate-limiting step in this process [30]. Both the film diffusion and pore diffusion processes may be therefore considered as rate-controlling steps.

3.7.2. Intraparticle diffusion model

To verify the possibility of both the film diffusion and the pore diffusion to be the rate-controlling steps, intraparticle diffusion model (Eq. (11)) was applied to the experimental data:

$$q_t = k_{id} \sqrt{t} + I \quad (11)$$

where k_{id} is the intraparticle rate constant and I represents the boundary layer effect [26]. The Eq. (11) predicts linear dependence of q_t upon $t^{1/2}$ with k_{id} as a slope of the line and I as an intercept (Fig. 10). It has been suggested by H_0 [31] that intercept of the plot of q_t vs. \sqrt{t} must be zero if the intraparticle diffusion is the sole rate-limiting step. Present investigations for the adsorption of fluoride on the nanocomposite gives positive value of the intercept ($I = 0.199$). It is therefore concluded that adsorption of fluoride on the nanocomposite follows mechanism in which film diffusion and pore diffusion are the rate-controlling steps.

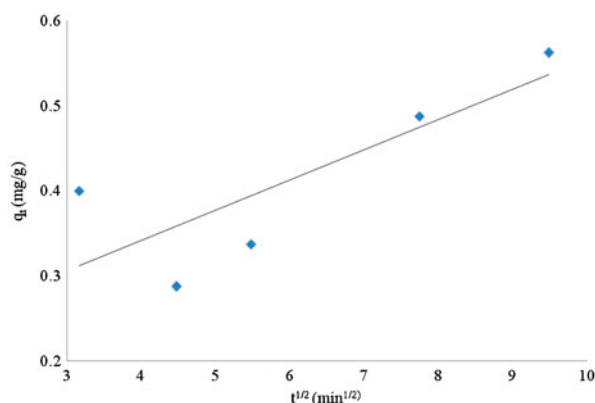


Fig. 10. Graph of intraparticle diffusion model for the removal of fluoride on the nanocomposite.

4. Conclusions

XRD pattern of MgAl_2O_4 synthesized by the co-precipitation method shows the single spinel phase with average crystallite size of 33 nm. TGA curve of nanocomposite confirms the successful incorporation of MgAl_2O_4 in the polymer network. The equilibrium data are well described by Langmuir model. Negative value of ΔG indicates that the adsorption of fluoride on the nanocomposite is spontaneous in nature. Non-linear plot of Bingham's model and non-zero intercept of intraparticle diffusion model gives the mechanism in which film diffusion and pore diffusion are the rate-controlling steps for adsorption of fluoride on the nanocomposite. Higher removal of fluoride (96%) shows that the nanocomposite can be used as an efficient adsorbent for the defluoridation of water particularly at lower fluoride concentration.

References

- [1] Y. Vijaya, A. Krishnaiah, Column adsorption and desorption studies of fluoride on perchloric acid cross-linked calcium alginate beads, *Eur. J. Chem.* 7 (2010) 265–270.
- [2] J.V. Kumar, M.E. Moss, Fluorides in dental public health programs, *Dent. Clin. North Am.* 52 (2008) 387–401.
- [3] S. Ayoob, A.K. Gupta, Fluoride in drinking water: A review on the status and stress effects, *Environ. Sci. Technol.* 36 (2006) 433–487.
- [4] P. Sehn, Fluoride removal with extra low energy reverse osmosis membranes: Three years of large scale field experience in Finland, *Desalination* 223 (2008) 73–84.
- [5] S. Dobaradaran, A.H. Mahvi, S. Dehdashti, D.R.V. Abadi, I. Tehran, Drinking water fluoride and child dental caries in Dashtestan, Iran, *Fluoride* 41 (2008) 220–226.
- [6] N. Mameri, A.R. Yeddou, H. Lounici, H. Grib, D. Belhocine, B. Bariou, Defluoridation of septentrional Sahara water of North Africa by electrocoagulation process using bipolar aluminium electrodes, *Water Res.* 32 (1998) 1604–1610.
- [7] A. Kass, Y. Gavrieli, A. Vengosh, A. Starinsky, The impact of freshwater and wastewater irrigation on the chemistry of shallow ground-water: A case study from the Israeli Coastal aquifer, *J. Hydrol.* 300 (2005) 314–331.
- [8] R.C.M. Meenakshi, Fluoride in drinking water and its removal, *J. Hazard. Mater.* 137 (2006) 456–463.
- [9] R. Aldaco, A. Garea, A. Irabien, Calcium fluoride recovery from fluoride wastewater in a fluidized bed reactor, *Water Res.* 41 (2007) 810–818.
- [10] J. Liu, Z. Xu, X. Li, Y. Zhang, Y. Zhou, Z. Wang, X. Wang, An improved process to prepare high separation performance PA/PVDF hollow fiber composite nanofiltration membranes, *Sep. Purif. Technol.* 58 (2007) 53–60.
- [11] S. Lahnid, M. Tahaikt, K. Elaroui, I. Idrissi, M. Hafsi, I. Laaziz, Z. Amor, F. Tiyal, A. Elmidaoui, Economic evaluation of fluoride removal by electro dialysis, *Desalination* 230 (2008) 213–219.
- [12] A.A.M. Daifullah, S.M. Yakout, S.A. Elreefy, Adsorption of fluoride in aqueous solutions using KMnO_4 -modified activated carbon derived from steam pyrolysis of rice straw, *J. Hazard. Mater.* 147 (2007) 633–643.
- [13] H. Paudyal, B. Pangepi, K. Inoue, H. Kawakita, K. Ohto, K.N. Ghimire, H. Harada, S. Alam, Adsorptive removal of trace concentration of fluoride ion from water by using dried orange juice residue, *Chem. Eng. J.* 223 (2013) 844–853.
- [14] V. Tomar, D. Kumar, A critical study on efficiency of different materials for fluoride removal from aqueous media, *Chem. Central J.* 7 (2013) 1–15.
- [15] S.P. Suriyaraj, T. Vijayaraghavan, P. Biji, R. Selvakumar, Adsorption of fluoride from aqueous solution using different phases of microbially synthesized TiO_2 nanoparticles, *J. Environ. Chem. Eng.* 2 (2014) 444–454.
- [16] V.S. Chauhan, P.K. Dwivedi, L. Iyengar, Investigations on activated alumina based domestic defluoridation units, *J. Hazard. Mater.* 139 (2007) 103–107.
- [17] S. Ayoob, A.K. Gupta, Insights into isotherm making in the sorptive removal of fluoride from drinking water, *J. Hazard. Mater.* 152 (2008) 976–985.
- [18] A.K. Yadav, C.P. Kaushik, A.K. Haritash, A. Kansal, N. Rani, Column adsorption and desorption studies of fluoride on perchloric acid cross-linked calcium alginate beads, *J. Hazard. Mater.* 128 (2006) 289–293.
- [19] M. Mahramanlioglu, I. Kizilcikli, I.O. Bicer, Adsorption of fluoride from aqueous solution by acid treated spent bleaching earth, *J. Fluorine Chem.* 115 (2002) 41–47.
- [20] D. Dayananda, V.R. Sarva, S.V. Prasad, J. Arunachalam, N.N. Ghosh, Preparation of CaO loaded mesoporous Al_2O_3 : Efficient adsorbent for fluoride removal from water, *Chem. Eng. J.* 248 (2014) 430–439.
- [21] S. Kurien, S. Sebastian, J. Mathew, K.C. George, Structural and electrical properties of nano-sized magnesium aluminate, *Ind. J. Pure Appl. Phys.* 42 (2004) 926–933.
- [22] Z.I. Zafar, M.A. Malana, H. Pervez, M.A. Shad, M. Khakwani, Synthesis and swelling kinetics of a cross linked pH-sensitive ternary copolymer gel system, *Polymer (Korea)* 32 (2008) 219–229.
- [23] S.M. Ghosh, M. Das, S. Ghatak, Microstructural characterization of amorphous and nanocrystalline boron nitride prepared by high energy ball milling, *Mater. Res.* 43 (2008) 1023–1031.
- [24] F. Renault, N. Morin-Crini, F. Gimbert, P.M. Badot, G. Crini, Cationized starch-based material as a new ion-exchanger adsorbent for the removal of Cl acid blue 25 from aqueous solutions, *Bioresour. Technol.* 99 (2008) 7573–7586.
- [25] M. Alkane, O. Demirbas, S. Celikcapa, M. Dogan, Sorption of acid red 57 from aqueous solution onto sepiolite, *J. Hazard. Mater.* B116 (2007) 135–145.
- [26] M. Malakootian, M. Moosazadeh, N. Yousefi, A. Fatehizadeh, Fluoride removal from aqueous solution by pumice: Case study on kuhbonan water, *African J. Environ. Sci. Technol.* 5 (2011) 299–306.

- [27] M.J. Iqbal, M.N. Ashiq, Adsorption of dyes from aqueous solution on activated charcoal, *J. Hazard. Mater.* B139 (2007) 57–66.
- [28] T. Sismanoglu, Removal of some fungicides from aqueous solution by the biopolymer chitin, *Colloid Surf. A* 297 (2007) 38–45.
- [29] A. Aygun, S. Yenisoy-Karakas, I. Duman, Production of granular activated carbon from fruit stones and nutshells and evaluation of their physical, chemical and adsorption properties, *Micropor. Mesopor. Mater.* 66 (2003) 189–195.
- [30] I.D. Mall, V.C. Sivastava, N.K. Agarwal, Removal of orange-G and methyle violet dyes by adsorption on to bagasse fly ash—Kinetic study and equilibrium isotherm analyses, *Dyes Pigm.* 69 (2006) 210–223.
- [31] Y.S. Ho, Removal of copper ions from aqueous solution by tree fern, *Water Res.* 37 (2003) 2323–2330.